Dynamics of electron solvation in $I^-(CH_3OH)_n$ clusters ($4 \leq n \leq 11$)

Ryan M. Young,[1] Margaret A. Yandell,[1] and Daniel M. Neumark[1,2,a)]
[1]*Department of Chemistry, University of California, Berkeley, California 94720, USA*
[2]*Chemical Sciences Division, Lawrence Berkeley National Laboratory, Berkeley, California 94720, USA*

(Received 8 December 2010; accepted 20 February 2011; published online 30 March 2011)

The dynamics of electron solvation following excitation of the charge-transfer-to-solvent precursor state in iodide-doped methanol clusters, $I^-(CH_3OH)_{n=4-11}$, are studied with time-resolved photoelectron imaging. This excitation produces a $I\cdots(CH_3OH)_n^-$ cluster that is unstable with respect to electron autodetachment and whose autodetachment lifetime increases monotonically from ~800 fs to 85 ps as n increases from 4 to 11. The vertical detachment energy (VDE) and width of the excited state feature in the photoelectron spectrum show complex time dependence during the lifetime of this state. The VDE decreases over the first 100–400 fs, then rises exponentially to a maximum with a ~1 ps time constant, and finally decreases by as much as 180 meV with timescales of 3–20 ps. The early dynamics are associated with electron transfer from the iodide to the methanol cluster, while the longer-time changes in VDE are attributed to solvent reordering, possibly in conjunction with ejection of neutral iodine from the cluster. Changes in the observed width of the spectrum largely follow those of the VDEs; the dynamics of both are attributed to the major rearrangement of the solvent cluster during relaxation. The relaxation dynamics are interpreted as a reorientation of at least one methanol molecule and the disruption and formation of the solvent network in order to accommodate the excess charge. © *2011 American Institute of Physics*. [doi:10.1063/1.3563720]

I. INTRODUCTION

How chemical environments stabilize excess charges is of critical importance in biology, solution phase chemistry, and condensed matter physics. The solvated electron is perhaps one of the best-studied species in this area as it is the simplest quantum solute[1,2] with only electronic degrees of freedom. Solvated electrons can be produced from the charge-transfer-to-solvent (CTTS) bands of solvated anions,[3] typically halide species such as iodide, I^-. Though most attention has been focused on CTTS dynamics in water,[4,5] solvated electrons have been produced from CTTS excitations in a variety of other solvents, such as ethylene glycol,[6] tetrahydrofuran,[7,8] acetonitrile,[9] and many alcohols, including methanol.[10] In the gas phase, iodide has no bound excited states and photoexcitation leads directly to detachment into the vacuum. However, upon solvation by only a few solvent molecules, an excited state can be observed as a broad feature in the electronic absorption spectrum of the gas-phase cluster.[11] Excitation then leads to ejection of the charge from the iodide onto the solvent network, which then begins to relax around it. Hence, time-resolved studies of halide-solvent clusters[12–14] provide complementary insights when compared with experiments performed in solution. In this paper, we investigate electron solvation dynamics in $I^-(CH_3OH)_n$ clusters subsequent to CTTS excitation.

Methanol is similar to water as it is polar and it can participate in hydrogen bonding, but it also has an aliphatic end more suited for nonpolar interactions. In many ways, it is the closest solvent to water and can be thought of as its "methylated" counterpart. Methanol differs significantly, however, as it can participate in only half as many hydrogen bonds. Its similarities and differences compared to water allow for a better understanding of how the local solvent environment affects electron solvation and solvent relaxation. To this end, numerous experimental[15–21] and theoretical[22–24] investigations have been carried out on the dynamics of electron solvation in methanol. For example, ultrafast transient absorption experiments have been utilized by Bradforth and co-workers[5,25] to probe the CTTS dynamics from iodide in water, methanol, and lower alcohols. By monitoring the absorbance of the nascent solvated electron, they find that the electron is ejected from the iodide into the primary solvent cavity, forming a contact pair with the neutral iodine during the first ~300 fs. From there, it either undergoes geminate recombination or diffuses out of the solvent cavity. The recombination and escape dynamics in methanol are both slower than those in water, which is explained in their model as a result of the higher viscosity of methanol.

As a complement to the work in solution, experiments on halide-solvent clusters examine electron solvation dynamics as a function of size and reveal details of the molecular processes behind charge transfer and subsequent stabilization.[11,12,26,27] Time-resolved photoelectron spectroscopy experiments on $I^-(CH_3OH)_n$ (n = 5–8) by Davis *et al.*[28] showed that after electron transfer, the excited state of the cluster is metastable, with the population decaying within ~22 ps for the largest cluster studied. The ultimate fate of the excess electron was attributed to "thermionic emission" or, more specifically, to vibrational autodetachment (VAD), as geminate recombination of the electron with the neutral

a)Author to whom correspondence should be addressed. Electronic mail: dneumark@berkeley.edu.

iodine would release enough energy to fracture the cluster which was not observed. However, the low energy electrons expected from autodetachment were not detectable with the magnetic bottle analyzer used in those experiments. Davis also noted the unique evolution of the shape of the photoelectron spectrum, which was markedly broader and more asymmetric than in similar experiments with other solvents. The asymmetry of the spectra was speculatively attributed to evaporative loss of either iodine or a solvent monomer or from the contribution of another state with a shorter lifetime. However, little was known at the time about the structure of the initial and final state geometries or the energetics of bare methanol cluster anions, so no definitive assignment could be made.

Recent experimental and theoretical investigations into methanol clusters have caused us to revisit the dynamics of $I^-(CH_3OH)_n$. Infrared (IR) predissociation studies on small ($n \leq 12$) $X^-(CH_3OH)_n$ clusters ($X^- = F^-$, Cl^-, I^-) by Lisy, Johnson, and co-workers,[27,29–31] and accompanying quantum chemical calculations[32] have provided the first structural probes of these clusters, in particular, probing whether the halide anion is solvated internally or resides at the surface of the cluster. The experiments find that the halide anion is hydrogen-bonded to one or more OH groups on adjacent methanol molecules. However, evidence for methanol–methanol binding is seen for clusters as small as $I^-(CH_3OH)_2$, indicating a propensity for the methanol molecules to bind to one another as opposed to binding to the halide and leaving the anion at the cluster surface. Interestingly, molecular dynamics simulations predict little or no enhancement of iodide at the liquid–vapor interface of bulk methanol[33,34] because the methanol surface is covered by hydrophobic methyl groups with the OH groups pointed inward; this situation differs substantially from water, which exhibits considerable iodide enhancement at its surface.[35]

Additional motivation for revisiting CTTS dynamics in $I^-(CH_3OH)_n$ clusters comes from recent experimental and theoretical work on $(CH_3OH)_n^-$ cluster anions. These clusters are, in essence, the final states expected in our CTTS experiments. Methanol cluster anions comprising 70–460 solvent molecules were studied in our research group by one-photon[36] and time-resolved[37] photoelectron imaging. The absence of anion clusters with fewer than 70 methanol molecules in the mass spectrum suggested that these smaller clusters were unstable on the time scale of our experiment. The one-photon studies demonstrated the existence of two distinct electron solvation motifs (isomers).[36] The first is a weakly-bound state (isomer II) that appears at higher ion source backing pressures. Isomer II clusters exhibit narrow photoelectron spectra which were assigned to clusters with surface-bound electrons. The other isomer (isomer I) is more strongly bound, with a broader photoelectron spectrum, and is favored at lower ion source backing pressures. We proposed that isomer I is the more "bulklike" state, possibly being internally solvated. Time-resolved experiments on this isomer[37] yielded internal conversion lifetimes that extrapolated reasonably well to the timescales from transient absorption experiments on electrons in bulk methanol by Thaller *et al.*[21] On the theoretical side, a new electron-methanol pseudopotential has recently been developed by Turi[24,38] and applied to large methanol cluster anions (n = 50–500). This work found diffuse, weakly-bound surface states with surface methyl groups oriented toward the excess electron, similar to the isomer II structure inferred from our photoelectron spectra.[36]

With better knowledge of the initial and final states, we reexamine here the dynamics of $I^-(CH_3OH)_n$ following CTTS excitation with time-resolved photoelectron imaging (TRPEI) over a larger size range (n = 4–11) than previously reported. Photoelectron imaging yields the photoelectron kinetic energy and angular distribution. As has been demonstrated for $I^-(H_2O)_n$ clusters,[39,40] the near-unity collection efficiency of charged particle imaging enables tracking of the autodetachment channel that cannot be observed with a magnetic bottle analyzer. We find this channel to be the dominant pathway for population decay for $I^-(CH_3OH)_n$ clusters, as $(CH_3OH)_n^-$ clusters are unstable in this size regime. Short time dynamics (100–400 fs) not previously observed are attributed to the electron associating with the solvent moiety immediately following excitation. The cluster response to this charge distribution can be monitored by the evolution of the photoelectron spectrum. The observed changes in the binding energy of the electron (3–20 ps) and the width of the spectrum (5–30 ps) are evidence for a major rearrangement of the solvent geometry near the halide and the excess electron.

II. EXPERIMENTAL

The femtosecond time-resolved photoelectron imaging apparatus has been described in detail elsewhere.[39] Briefly, argon carrier gas at ~20 psig was flowed over reservoirs of liquid methanol and methyl iodide at room temperature into a pulsed solenoid valve[40] operating at 100 Hz. The resulting pulsed jet then passed through a ring electrode ionizer. Secondary electrons from the ionization process formed I^- via dissociative electron attachment to CH_3I, which could either be picked up by methanol clusters in the jet or act as a nucleation site for cluster formation. The anion beam was injected into a Wiley–McLaren time-of-flight mass spectrometer,[41] configured so that only ions of the desired mass interacted with the pump and probe laser pulses. Additional size selectivity was accomplished by an electrostatic switch at the entrance to the interaction region pulsed at the appropriate time. Ejected photoelectrons were accelerated by velocity-map imaging[42] onto a pair of chevron-mounted 75 mm microchannel plates coupled to a phosphor screen. Intensified images were collected at 30 Hz with a CCD camera and four-way symmetrized to ensure homogeneity.

Images were reconstructed using the BASEX method[43] for photoelectron kinetic energy (eKE) spectra or the pBASEX method[44] for the photoelectron angular distributions (PADs). The PADs were fit to an even series of Legendre polynomials:[45]

$$I(\theta, \mathrm{eKE}; n) = \frac{\sigma_{\mathrm{total}}}{4\pi}[1 + \beta_2(\mathrm{eKE}; n) P_2(\cos\theta) + \beta_4(\mathrm{eKE}; n) P_4(\cos\theta)], \quad (1)$$

where I is the intensity, θ is the angle between the photoelectron wave vector and the laser polarization, n is the cluster size, σ_{total} is the total photodetachment cross section, and

$\beta_{2,4}$ are anisotropy parameters which contain information about the excess electron's angular momentum.

Pump and probe laser pulses were generated in a commercial Ti:sapphire oscillator and then amplified by chirped-pulse multipass amplification (KM Labs Griffin oscillator/Dragon amplifier), resulting in pulses of 35 fs duration (full width at half maximum, FWHM) at 790 nm (1.57 eV). 75% of this light was directed into a third-harmonic generator, yielding pulses at 263 nm (4.71 eV) with 30 μJ/pulse to be used to excite the CTTS transition. The remaining fundamental was attenuated and used as the probe pulse, with a pulse energy at the entrance to the vacuum chamber of 120–200 μJ/pulse. Time resolution at the vacuum chamber was measured *in situ* by above threshold detachment of iodide as ~80 fs.

III. RESULTS

TRPEI was carried out for $I^-(CH_3OH)_n$ clusters with $n = 4$–11 and their deuterated analogs (–*d*1) and (–*d*4). Figure 1 shows the time-resolved photoelectron spectrum for $I^-(CH_3OH)_4$, with eKE decreasing from left to right and pump–probe delay increasing nonlinearly from front to back. Four prominent features are seen: an intense, time dependent signal at eKE ~0 (feature A), a peak from 1.5–1.8 eV that appears near the zero of pump–probe delay (B), a broad peak around 0.25 eV (C), and a low-intensity feature around 1.5 eV which shows no time-dependence (D). These last two features are only seen for $n = 4$. Figure 2 shows TRPE spectra for $I^-(CH_3OH)_7$; this spectrum is representative of cluster sizes with $n \geq 5$ for each isotopomer. They are similar to those previously presented by Davis,[28] but the sharp, intense feature (A) near eKE = 0 was not seen in that work owing to the poor transmission of the magnetic bottle analyzer for very low eKE. Feature A dominates the spectra for all cluster sizes $n \geq 5$ but becomes less intense overall for the largest cluster sizes as the CTTS band blue-shifts away from 263 nm. Integrated intensities of features A and B are shown in the insets of Figs. 1 and 2.

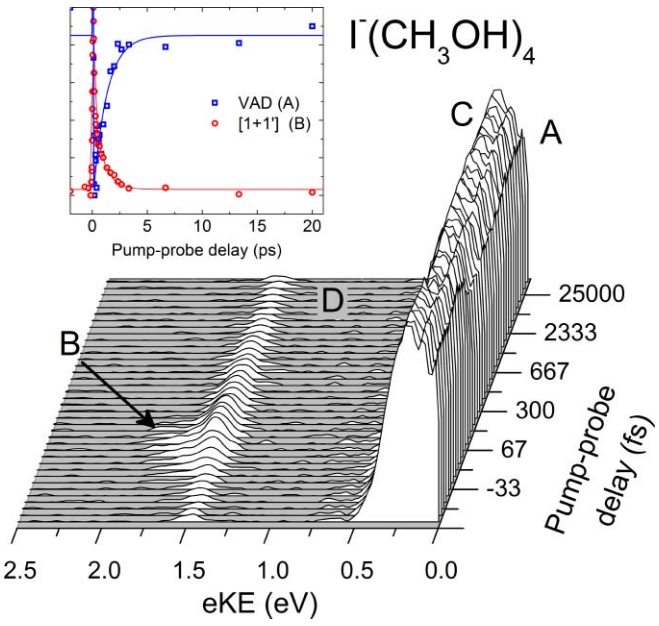

FIG. 1. Time-resolved photoelectron spectrum for $I^-(CH_3OH)_4$ with pump–probe delay increasing nonlinearly from front to back. Feature A is due to vibrational autodetachment (VAD), feature B is the resonant two-photon [1+1] signal, feature C is from UV direct detachment to the $^2P_{3/2}$ state of iodine, and feature D is from 4-photon IR detachment to the $^2P_{3/2}$ state. Normalized intensities of Features A (blue) and B (red) are shown in the inset, with fits shown as solid lines.

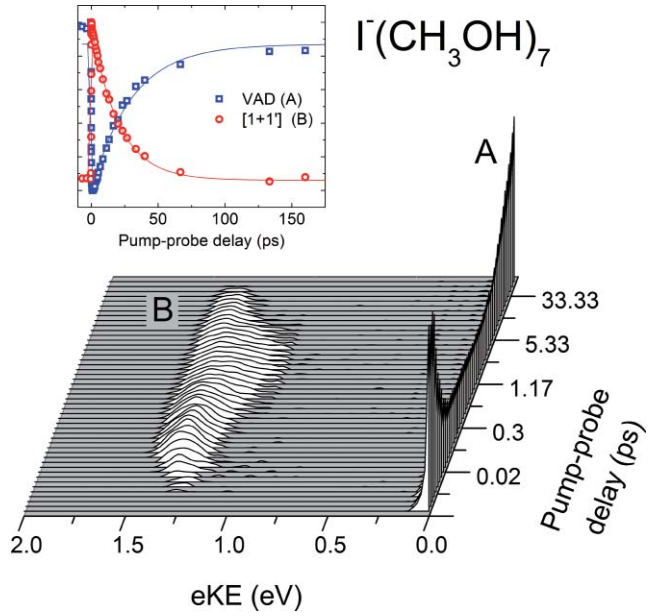

FIG. 2. Time-resolved photoelectron spectrum for $I^-(CH_3OH)_7$ with pump–probe delay increasing nonlinearly from front to back. Feature A is due to vibrational autodetachment; feature B is the resonant two-photon [1+1] signal. Normalized intensities of features A (blue squares) and B (red circles) are shown in the inset, with fits shown as solid lines.

For all cluster sizes, features A and B exhibit a strong and complementary dependence on the pump–probe delay. The intensities of both features change abruptly near the zero of pump–probe delay, t_0. Feature A is depleted by the probe pulse from its pump–only value at negative time delays, whereas feature B is not seen until the pump and probe pulses overlap. Both features then return more slowly to their initial values on a time scale that increases with cluster size, ranging from 1–2 ps for $n = 4$ to nearly 100 ps for $n = 11$. For $n \geq 6$, features A and B reach their respective minimum or maximum intensities 1–3 ps after the cross-correlation time of the two laser pulses.

Based on our previous work on $I^-(H_2O)_n$ and $I^-(CH_3CN)_n$ clusters,[46,47] we assign feature A to VAD of the $I^-(CH_3OH)_n$ clusters after pump excitation. Likewise, feature B is assigned to the [1+1′] pump–probe signal from the excited state of the cluster. These assignments explain the complementary time-dependence of features A and B, since the excited state either undergoes autodetachment or is photodetached by the probe pulse.[46,47] For all sizes studied here, both the peak and width of the eKE distribution for feature B change significantly with pump–probe delay, with the extent of this variation changing with cluster size. Partial (–*d*1) and full (–*d*4) deuteration result only in small effects on the time-dependent intensities, binding energies, and spectral shapes.

The detailed time-dependence of features A and B is explored in Sec. IV.

For $n = 4$, feature C is also seen with only the UV pulse and is due to direct detachment of I^- to the $^2P_{3/2}$ state of iodine. Similarly, feature D is seen with only the infrared pulse and is attributed to 4-photon IR detachment of I^- to the $^2P_{3/2}$ state of neutral iodine, shifted to slightly higher binding energy due to the ponderomotive effect of the high-intensity laser field.[48] A small ridge on the low eKE side of feature C is at approximately the correct energy for 3-photon detachment to the $^2P_{3/2}$ state. These features are not seen for larger cluster sizes or at lower pulse energies.

Feature A is a one-photon process and can be fit with a single anisotropy parameter. For the sizes studied here, the feature was symmetric and β_2 was ~0 for all delays. The pump–probe feature B was fit to Eq. (1). For cluster sizes with sufficient signal-to-noise, the two-photon anisotropy parameter β_4 was observed to be close to zero (–0.1 to 0.3) at all pump–probe delays, while β_2 showed marked temporal evolution. The sensitivity of the pBASEX algorithm to both signal levels and to noise makes the time-dependent feature more difficult to fit, but general observations can be made about the anisotropy near t_0 and very long pump–probe delays. The images begin with a significant anisotropy for feature B ($\beta_2 \sim 0.7-1.0$) and then become more isotropic ($\beta_2 \sim 0-0.4$) before the signal fades. No obvious size-dependent trends in the anisotropy parameters were observed.

IV. ANALYSIS

In this section, we analyze the temporal evolution of the photoelectron spectra in detail. Time-dependent intensities for each feature are fit to retrieve the lifetime of the excited cluster, and the eKE distribution itself is fit at each delay to extract vertical detachment energies (VDEs) and the FWHM of the excited state feature.

First, we focus on the lifetime of the excited state and the autodetachment process. The intensities of features A and B are determined by integrating over the respective range of the eKE distribution at each time delay. The resultant intensities are then fit to Eq. (2), representing the convolution of a Gaussian instrumental response function of temporal width σ with the sum of (i) a multiexponential function characterized by time constants τ_{Xi} where X is either A or B, (ii) a delta function centered at t_0 (to account for coherence artifacts during the cross-correlation time), and (iii) an offset, I_0:

$$I_X = e^{-t^2/\sigma^2} * \begin{cases} I_0, & t < t_0 \\ I_0 + a_0\delta(t - t_0) \\ \quad + \sum_i a_i \exp[(t - t_0)/\tau_{Xi}], & t \geq t_0 \end{cases}, \tag{2}$$

where $i = 1$ for $n = 4$, 5 and $i = 1$, 2 for larger clusters. The time resolution of the apparatus is given by $\tau_{FWHM} = 2\sigma\sqrt{\ln 2} = 70$–$90$ fs. For clusters larger than $n = 5$, the integrated intensity of the excited state feature rises and falls in a bi-exponential fashion; the rise time τ_{B1} is around 1 ps for $6 \leq n \leq 11$.

Features A and B can be described by the same equation with opposite signs for the coefficients a_i; the recovery of feature A is systematically slower than the decay of feature B by a few percent, though within the error bars. This small discrepancy is attributed to the intrinsic difficulty in measuring small changes in feature A atop a large background. Hence, we report the time constants τ_{B1} and τ_{B2} as the lifetimes of the excited clusters for $n \leq 5$ and $n \geq 6$, respectively. These time constants are listed in Table I.

Excited state VDEs are determined by fitting an asymmetric Gaussian function to the eKE spectrum over the range of feature B to monitor the time-dependent energetics of the excited state for each cluster size and at each pump–probe delay. The kinetic energy profile for cluster n is fit to

$$I_n(\text{eKE}; t) = \begin{cases} I_0 + be^{-[\text{eKE}-E_0(t)]^2/w_1^2(t)}, & \text{eKE} < \text{E}_0 \\ I_0 + be^{-[\text{eKE}-E_0(t)]^2/w_2^2(t)}, & \text{eKE} \geq \text{E}_0 \end{cases}, \tag{3}$$

where b is a scaling parameter, E_0 is the peak of the eKE distribution, and w_1 and w_2 are the width parameters on either side of the peak. Equation (3) is a phenomenological lineshape that has been observed previously for halide-solvent clusters.[47] The FWHM of the kinetic energy profile is $(w_1 + w_2) \times \sqrt{\ln 2}$. For $n = 4$ only, where direct detachment leading to features C and D competes with CTTS excitation, the eKE spectrum at $\Delta t = -1$ ps is first subtracted before fitting to avoid contamination. Figure 3 shows the eKE distribution and accompanying fits for $I^-(CH_3OH)_7$ at various delays, showing how both the peak energy and the width of the spectrum change significantly over time.

The time-dependent peak of the eKE distribution, $E_0(t)$ yields the vertical detachment energy:

$$\text{VDE}(t) = h\nu - E_0(t). \tag{4}$$

VDEs versus delay are shown for $I^-(CH_3OH)_7$ in Fig. 4. Following CTTS excitation, the VDEs quickly fall to a minimum value, VDE_{min}, during the first 100–400 fs (t_{min}) with no clear size dependence over the range studied here. For $n \geq 5$, over the next ~1–3 ps, the VDE rises to a maximum, VDE_{max}, before falling again for the remainder of the excited state lifetime, typically approaching a value lower

TABLE I. Timescales for excited state lifetime, VDE, and FWHM dynamics (in picoseconds). Values represent averages over data sets and errors represent the standard deviation of the mean. Only population information is available for $n = 4$ due to the short lifetime of the cluster and for $n = 11$ due to signal levels.

Cluster size (n)	Lifetime	VDE		FWHM	
	τ_{B2}	t_{max}	τ_2	T_{max}	T_2
4	0.80 ± 0.07[a]	n/a	n/a	n/a	n/a
5	4.10 ± 0.02[a]	1.5 ± 0.2	3.1 ± 0.3	1.4 ± 0.2	5.6 ± 0.3
6	9.40 ± 0.52	1.8 ± 0.2	4.5 ± 1.1	2.8 ± 0.3	8.0 ± 2.9
7	19.6 ± 0.49	1.7 ± 0.2	7.5 ± 1.4	2.7 ± 0.3	7.5 ± 1.1
8	32.6 ± 0.44	3.5 ± 0.3	9.5 ± 0.3	2.4 ± 0.3	9.3 ± 1.0
9	49.7 ± 0.79	3.6 ± 0.3	16.7 ± 3.9	4.4 ± 0.7	23 ± 9.3
10	70.9 ± 2.59	2.4 ± 0.7	20.1 ± 7.6	5.2 ± 0.3	30 ± 12
11	85.5 ± 6.30	n/a	n/a	n/a	n/a

[a]Lifetime given by τ_{B1}.

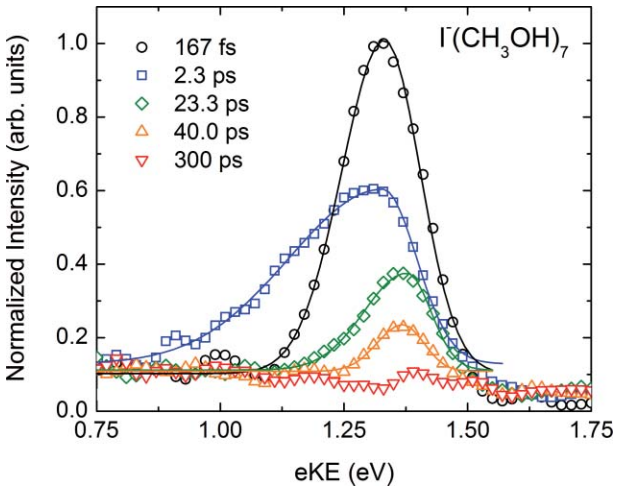

FIG. 3. Photoelectron spectra at the following pump–probe delays for $I^-(CH_3OH)_7$. Black circles: 167 fs; blue squares: 2.3 ps; green diamonds: 23.3 ps; orange upward triangles: 40.0 ps; red downward triangles: 300 ps. Spectra at each delay are normalized to the peak intensity of the spectrum at $t = 167$ fs.

than the initial local minimum at t_{min}. Time-dependent VDEs after VDE_{min} can be fit to a bi-exponential process:

$$VDE_n(t) = VDE_n(\infty) + c_2^{(n)} e^{-(t-t_0)/\tau_1^{(n)}} + c_3^{(n)} e^{-(t-t_0)/\tau_2^{(n)}}, \quad (5)$$

where τ_i is the relaxation time for each term and $VDE_n(\infty)$ is an estimate of the asymptotic VDE. The second term applies to the rise ($c_2 < 0$), while the third describes the decrease in VDE ($c_3 > 0$). The increase to maximum VDE takes place on a timescale τ_1 ranging from 0.7–2 ps, generally increasing with cluster size. The pump–probe delay t_{max} corresponding to VDE_{max} is taken directly from the spectra. The relaxation time τ_2 toward $VDE(\infty)$ increases from 3 to 20 ps from $n = 5$ to 10. The decay of the excited state signal leads to the increased errors associated with the fitting of the long-time tails of the exponential decay. The time constants t_{max} and τ_2 are listed in Table I, while VDE_{min}, VDE_{max}, and $VDE(\infty)$ for each cluster are given in Table II.

While the relaxation times and $VDE(\infty)$ are taken from the least-squares fitting, changes in the VDE, ΔE_i ($i = 1$–3), are taken directly from the spectra and are shown graphically in Fig. 4. The initial change in energy between the first appearance of the excited state and VDE_{min}, $\Delta E_1 = VDE_{min} - VDE(0)$, becomes more pronounced with cluster size, varying from –40 meV at $n = 5$ to –115 meV for $n = 11$. $\Delta E_2 = VDE_{max} - VDE_{min}$ ranges from +45 to +165 meV over these sizes, and the long-time relaxation, $\Delta E_3 = VDE(\infty) - VDE_{max}$, varies from –60 to –220 meV, generally decreasing with cluster size. There is no strong isotope effect observed. Energy changes are listed in Table II and are shown in Fig. 5.

The width of feature B changes significantly with pump–probe delay, as can be seen in Figs. 1–3. After the excited state is first populated, the width of this feature rises to a maximum (as much as FWHM = 550 meV for $n = 11$); the corresponding delay time T_{max} ranges from 1–5 ps. The width then decreases as the excited state decays. The width at each pump–probe delay can be fit to

$$FWHM_n(t) = FWHM_n(\infty) + d_2^{(n)} e^{-(t-t_0)/T_1^{(n)}} + d_3^{(n)} e^{-(t-t_0)/T_2^{(n)}}, \quad (6)$$

where T_1 and T_2 describe the rise ($d_2 < 0$) and fall ($d_3 > 0$) times of the spectral width, respectively. The FWHM of $I^-(CH_3OH)_7$ at each delay is also shown in Fig. 6 alongside the VDE to show their similar dynamics. As shown in the figure, the maximum width of the [1+1′] feature is reached slightly after VDE_{max}; this is seen for all cluster sizes. The time constants T_{max} and T_2 are listed in Table I.

Figure 7 compares the time-dependent FWHM of feature B in representative halide clusters with CH_3OH, H_2O, and CH_3CN.[46,47] In all three solvents, the spectra broaden during the first 1–2 ps. However, for the latter two solvent species, the spectra rapidly narrow after only a few ps and their width remains constant throughout the remainder of the experimental window. In methanol, this decrease from maximal width occurs over a much longer timescale, as long as 30 ps for $n = 10$. The origin of this difference is considered in Sec. V.

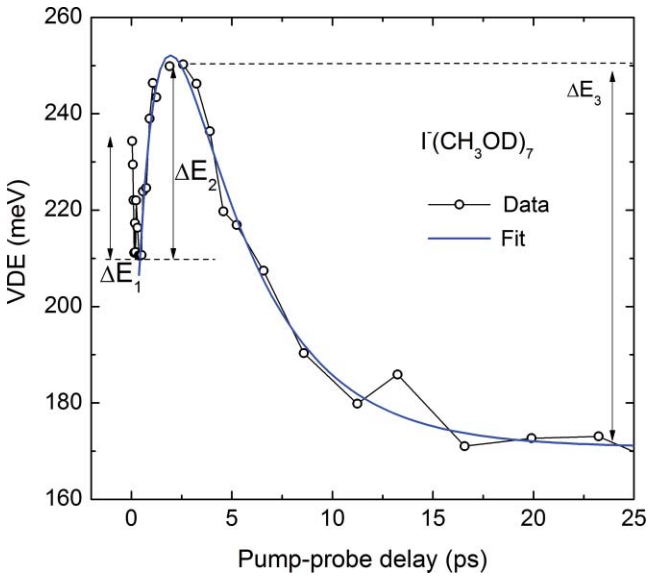

FIG. 4. VDE as a function of pump–probe delay for $I^-(CH_3OD)_7$ showing ΔE_1, ΔE_2, and ΔE_3.

V. DISCUSSION

In these experiments, the pump pulse ejects an electron from the iodide anion onto nearby solvent molecules, creating a cluster comprising several methanol molecules, an excess electron, and a neutral iodine atom. The initial configuration of the methanol molecules is set up to stabilize the iodide anion, and, as discussed below, significant rearrangement is expected to best accommodate the neutral iodine atom and excess electron. However, this accommodation is quite short-lived, because the electron leaves the cluster on a time scale varying from ~1–85 ps over the cluster size range studied here. The TRPE spectra present a wealth of information that can shed light on these dynamics. The integrated intensities of

TABLE II. VDEs at various time delays and associated changes for each cluster size for nondeuterated methanol, in meV. Values represent averages over data sets and errors represent the standard deviation of the mean.

Cluster size (n)	VDE(0)	VDE_{min}	VDE_{max}	VDE(∞)	ΔE_1	ΔE_2	ΔE_3
5	130 ± 10	90 ± 5	140 ± 10	80 ± 5	–40 ± 10	50 ± 15	–60 ± 10
6	195 ± 15	140 ± 10	185 ± 10	115 ± 25	–55 ± 15	45 ± 10	–70 ± 20
7	250 ± 5	200 ± 5	260 ± 15	170 ± 10	–50 ± 10	60 ± 20	–90 ± 10
8	330 ± 20	230 ± 15	330 ± 15	210 ± 10	–100 ± 30	100 ± 25	–120 ± 25
9	325 ± 10	235 ± 15	375 ± 10	170 ± 10	–90 ± 25	140 ± 30	–205 ± 20
10	345 ± 30	255 ± 15	410 ± 20	190 ± 50	–90 ± 15	155 ± 15	–220 ± 50
11	450 ± 50	335 ± 30	500 ± 50	320 ± 30	–115 ± 50	165 ± 50	–180 ± 50

features A and B yield the population dynamics of the excited state, specifically the lifetime of the nascent anionic methanol cluster created by the pump pulse. The time-varying vertical detachment energy and width of feature B probe the response of the $I^-(CH_3OH)_n$ cluster to the ejection of an electron from the iodide anion. Each of these quantities and their evolution with time and cluster size provide insight into how small methanol clusters accommodate an excess charge. Comparison of these results with those obtained for iodide clustered with other solvents reveals significant differences in the overall dynamics.

A. Population dynamics

The "excited state" of the $I^-(CH_3OH)_n$ clusters in these experiments approximately corresponds to charge transfer from the anion to the solvent network. After CTTS excitation, the electron is associated with the methanol cluster moiety in a perturbed, unequilibrated geometry. Bare methanol clusters have been shown to support anion states for clusters only as small as $n = 71$, well beyond the size range studied here.[36] In the absence of a stable final state, the excess electron in the $I^{\cdots}(CH_3OH)_n^-$ cluster created by the pump pulse cannot be supported and will autodetach. This interpretation is supported by the observation that the decay of the pump–probe signal, feature B, and recovery of the autodetachment signal, feature A, occur on essentially the same time scale, as discussed in Sec. IV. The integrated intensity of feature B and the depletion of feature A both represent the population of the excited state created by the pump pulse, so the two signals exhibit complementary temporal character. Direct observation of this channel and its complementary nature to feature B allows us to fully account for the electron population after CTTS excitation. In the previous study by Davis, the fate of the electron could only be inferred from the data but could not be conclusively determined. Here, we can confirm the mechanism for the ultimate decay of the excess electron and can unequivocally say, for example, that it does not occur by recombination with the iodine atom.

The decay dynamics in this experiment are very different from those in our work on bare methanol cluster anions.[37] In those experiments, the excess electron associated with the methanol cluster is electronically excited, and decay of the excited state occurs by rapid (150–300 fs) internal conversion back to the ground electronic state of the anion, not by autodetachment. Here, in contrast, the perturbed methanol cluster anion created by CTTS excitation can be considered to be in its electronic ground state, so rapid internal conversion to

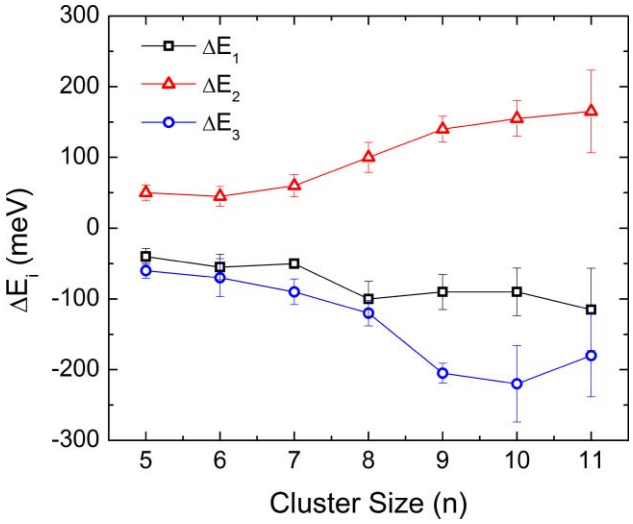

FIG. 5. Changes in vertical detachment energies as a function of cluster size: $\Delta E_1 = VDE_{min} - VDE(0)$ is shown as black squares, $\Delta E_2 = VDE_{max} - VDE_{min}$ is shown as red triangles, and $\Delta E_3 = VDE(\infty) - VDE_{max}$ is shown as blue circles. See text for details.

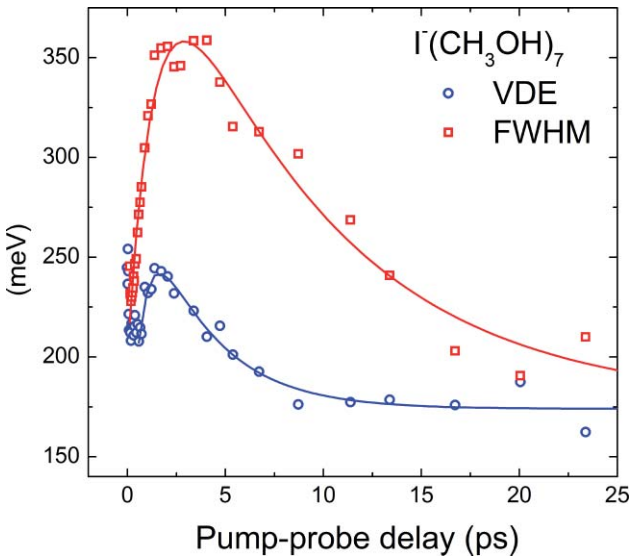

FIG. 6. VDE (blue circles) and FWHM (red squares) as a function of pump–probe delay for $I^-(CH_3OH)_7$.

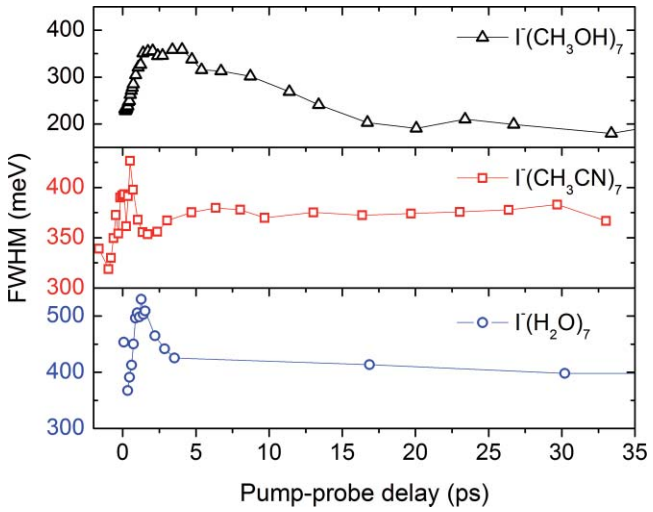

FIG. 7. Spectral FWHM for the excited state feature of the $n = 7$ cluster of iodide-doped methanol (black triangles), acetonitrile (red squares), and water (blue circles).

a lower state is not possible. For smaller clusters, $n < 6$, only a single decay constant is needed to fit the integrated intensities. Larger clusters ($n \geq 6$) show a delayed rise with a time constant on the order of 1 ps. This delayed rise is commensurate with early evolution of the VDE and peak width that are discussed in more detail in Sec. V B. It most likely arises from rapid changes in the photodetachment cross section as the excess electron starts interacting more with the solvent network and less with the iodine atom.

The thermionic emission rate should depend on the initial cluster temperature, which we estimate to be 100–150K based on the evaporative ensemble model.[49] It would be of interest to perform these experiments on ions that have been actively cooled to much lower temperatures,[50] but we have not systematically varied the temperature thus far. The lifetimes measured here are in good agreement with those reported by Davis, with the exception of $n = 8$, the largest cluster considered in that work, for which they obtained a lifetime of 22 versus 33 ps here. Owing to the improved signal-to-noise in the current experiment, and the observation that the newer value fits well within the size trend of the other clusters studied here (a larger range), we consider the new value to be more accurate.

The excited state lifetimes in these clusters as measured by decay of the pump–probe signal are much shorter than in $I^-(H_2O)_n$ and $I^-(CH_3CN)_n$,[28,46,47] but are comparable with lifetimes in similarly-sized $I^-(NH_3)_n$ clusters.[51] For example, the analogous lifetimes in $I^-(H_2O)_7$ and $I^-(H_2O)_{10}$ are 300 ps and least 3 ns, respectively. These differences may reflect the fact that $(H_2O)_n^-$ and $(CH_3CN)_n^-$ clusters are stable in this size range,[52,53] whereas $(CH_3OH)_n^-$ and $(NH_3)_n^-$ clusters are not.[54]

B. VDEs and peak widths

VDEs directly measure the difference in energy between the anion and neutral states at the instantaneous nuclear geometry as the cluster relaxes. These values show the same characteristics for all cluster sizes larger than $n \geq 5$, with individual values summarized in Tables I and II. The excited state lifetime of the $n = 4$ cluster is too short for any significant relaxation to occur, and is not discussed further. The fast decrease in VDE, ΔE_1, shown in Figs. 4 and 6, is complete after the first 100–400 fs. It is unlikely that significant rearrangement of the cluster occurs this rapidly. Thus, we attribute this portion of the relaxation to the electron interacting with both the solvent cluster and the iodine atom, forming the cluster analog of the "contact pair" that is proposed to form in the bulk. This fast change in the electron wavefunction contributes to the modulation in the photodetachment cross section observed in the early stages of the population dynamics. This modulation was not seen in the study by Davis but has been seen in studies of other halide-solvent clusters.[46,47]

Similar to the situation in iodide-water clusters, the subsequent change in energy ΔE_2 is attributed to the solvent response to the newly established charge distribution. However, in $I^-(H_2O)_n$ clusters, the longer time modulation ΔE_3 was ~–50 meV, independent of cluster size, whereas in $I^-(CH_3OH)_n$ clusters, ΔE_3 generally increases in magnitude with cluster size, from –30 to –220 meV over the size range considered here. The constant ΔE_3 in $I^-(H_2O)_n$ clusters was attributed to the loss of the iodine atom from the water cluster anion, to which it is only weakly bound,[55] but here it seems unlikely that loss of an iodine atom is solely responsible for the strongly size-dependent ΔE_3 values in $I^-(CH_3OH)_n$ clusters. Instead, we attribute these longer-time dynamics to solvent reorganization that destabilizes the anion relative to the neutral cluster.

The changing nature of the lineshape of feature B is also shown in Fig. 6 and the top panel of Fig. 7. In photoelectron spectra where no vibrational structure is resolved, peak widths are dictated by the Franck–Condon factors reflecting the nuclear wavefunction overlap of the anion and neutral states; larger displacements of the anion geometry from the equilibrium geometry of the neutral yield more vibrational activity upon photodetachment and hence broader peaks. Therefore, the width of feature B allows us to track the anion cluster geometry in relation to that of the neutral. This feature is widest around 2–5 ps, indicating maximal displacement from the neutral equilibrium geometry, and then narrows at longer times, indicating that the anion solvent configuration is approaching the geometry of the neutral methanol cluster.

Figure 8 shows a set of one dimensional potential energy curves that are consistent with our time-dependent VDEs and peak widths. These curves are loosely based on theoretical and experimental results on neutral[56,57] and anionic[38,58] methanol clusters, as well as halide-doped methanol clusters.[27,29–31] The x-axis represents the angle between the C–O bond of a solvent molecule (the average OH dipole direction) and the cluster center. The minimum energy geometry of the anion has one or more OH groups directed at the I^- ion ($\theta_{CO} \sim 180°$). Vertical excitation accesses the anion charge-transfer state. Both this state and the neutral methanol cluster have their lowest energy structures with the OH groups directed inward, maximizing the number of hydrogen bonds, so both of these surfaces will have minima at $\theta_{CO} \sim 0°$. Due to

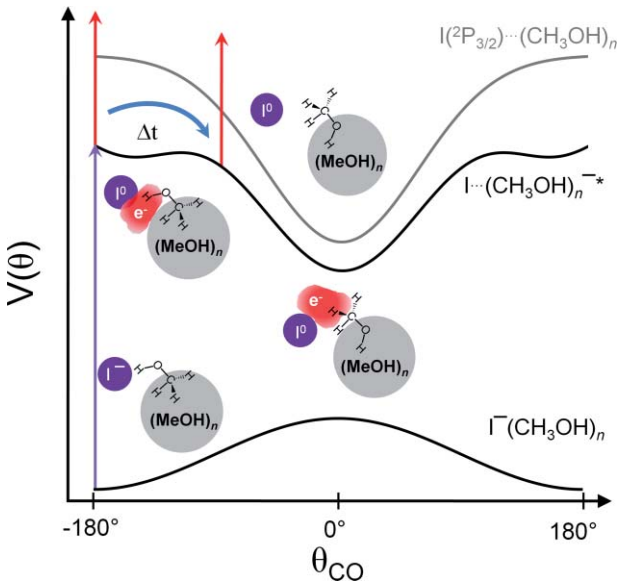

FIG. 8. Schematic potential energy surfaces for $I^-(CH_3OH)_n$ with associated geometries inferred from the spectra. Motion of one methanol molecule is shown for simplicity; the remaining solvent moiety is depicted as $(MeOH)_n$. See text for details.

the attractive nature of the $OH\cdots e^-$ interaction (~90 meV),[58] the anion surface may have a shallow minimum where the hydroxyl group is directed toward the electron center of mass. However this is not the global minimum, as the hydrogen bonds in methanol are each around 200 meV,[59] leading to the deeper well at $\theta_{CO} \sim 0°$. The reorientation of only one methanol is shown for simplicity, although the actual dynamics presumably involve collective solvent motion.

These curves, as drawn, are consistent with the salient features of our data. Specifically, the gap between the excited anion and neutral (the VDE of feature B) first increases then rapidly decreases as the cluster relaxes along the reaction coordinate, explaining the positive value of ΔE_2 and the negative value of ΔE_3. In addition, the initially prepared excited anion state lies above the minimum of the neutral curve, so autodetachment is energetically possible. In this one-dimensional picture, the widths of the photoelectron peaks are determined by the relative slopes of the potential energy curves at a given angle (the "reflection" principle of photodissociation[60]). Here again, these curves show that the width will increase to a maximum before decreasing again as θ_{CO} approaches 0°. We emphasize, however, that the curves in Fig. 8 are drawn to show that a simple and reasonable one-dimensional picture can explain our data; electronic structure calculations are needed to validate them.

The timescales observed in these experiments are in keeping with the proposed mechanism. Specifically, one expects those CH_3OH molecules with their OH bonds initially oriented toward the iodide at the surface of the cluster to undergo a half-rotation, resulting in more hydrogen bonds with other solvent molecules. A lower bound for the time associated with this rotation can be estimated as half of the $J = 1$ end-over-end rotational period for free methanol under the rigid rotor approximation for an asymmetric top,[61] which is ~9–10 ps. This motion will be hindered and slowed due to interactions with the other methanol molecules in the cluster, especially if the hydrogen bonds in the remainder of the cluster need to be broken in order to accommodate the additional contribution to the solvent network.

This relaxation mechanism is quite different than that proposed for halide-water clusters. $I^-(H_2O)_n$ clusters have been predicted to solvate iodide on their surface until at least n ~55.[62] Excess electrons in water clusters have been shown to exist in a variety of binding motifs,[50,63] with surface-bound states dominating at smaller sizes.[64] However, in contrast to methanol clusters, these surface-bound electrons interact with free OH bonds at the cluster surface. Methanol's ability to form only one hydrogen bond makes the energetics of the $OH\cdots e^-$ and $OH\cdots O$ interaction much more important in methanol than in water. Hence, relaxation of the solvent network certainly occurs upon CTTS excitation of $I^-(H_2O)_n$ clusters, but with less disruption to the cluster geometries compared to methanol clusters, as indicated by the constant widths at longer times of the excited state photoelectron spectra of $I^-(H_2O)_n$ clusters (see Fig. 7). In a similar vein, there is reasonably strong evidence that both iodide[65,66] and excess electrons[53,67–69] are internally solvated in $I^-(CH_3CN)_n$ and $(CH_3CN)_n^-$ clusters, respectively. Thus, both the initial and final states lie within the same solvent cavity, again reducing the extent of solvent reorientation needed upon excitation of $I^-(CH_3CN)_n$ clusters. Despite being chemically similar to both water and acetonitrile, the ability of methanol to both hydrogen bond and to stabilize a charged species with its methyl terminus cause it to have significantly different dynamics than either solvent.

C. Comparison to larger systems

A key question raised by these cluster studies is how the energetics and dynamics observed here correlate with those seen larger methanol cluster anions and with electrons in liquid methanol. We first compare the long-time VDEs measured here to the those seen in one-photon PE spectra of $(CH_3OH)_n^-$ clusters. As the cluster size increases, the binding energy of the nascent methanol cluster anion should increase, eventually approaching that of the appropriate stable cluster anion isomer. As seen in Table II, VDE(∞) does increase with cluster size and by $n = 11$ it is 320 meV, already larger than the VDE of 190 meV of $(CH_3OH)_{71}^-$ isomer II, the smallest isomer II cluster seen previously.[36] It thus appears that in the current work, the excess electron in the asymptotic cluster configuration (i.e., just prior to autodetachment) is more tightly bound than in an isomer II cluster.

A similar picture arises from the photoelectron angular distribution, where we observe feature B to have a sizeable anisotropy (~0.7–1.0) near t_0 that becomes much more isotropic prior to its decay. Our previous one photon study on large methanol cluster anions (n ~70–460) found smaller anisotropy parameters (β_2 ~0.25–0.16) for the more tightly bound isomer I clusters, while higher values (β_2 ~0.90–0.72) were seen for isomer II clusters.[36] Hence, while there is a significant difference between clusters of 70+ and clusters of 10 molecules, the photoelectron angular distributions also suggest that isomer II clusters are not the appropriate asymp-

totic limit in the $I^-(CH_3OH)_n$ experiments. This is not to say that the picture of solvent reorientation in Fig. 8 is incorrect, instead the implication is that the excess electron interacts more strongly with the solvent network in these clusters than in the very diffuse surface state of an isomer II cluster.

It would be of considerable interest to extend the $I^-(CH_3OH)_n$ experiments to much larger clusters to see if the long-time VDEs approached those of isomer I methanol cluster anions. This would provide for a continuous evolution to the structure of the solvated electron in liquid methanol whose suggested structure is for the OH groups of the alcohol to be directed toward the electron's center of mass.[19,22,70]

Time-resolved experiments[25] on photodetachment of I^- in bulk methanol and related theoretical treatments[71,72] indicate that CTTS excitation leads to formation of an $I{:}e^-$ "contact pair" on a time-scale of 200–300 fs. The newly formed electron can undergo either diffusive escape to form a solvated electron or geminate recombination with the iodine atom.[5,25,73] Diffusion is not applicable to an isolated cluster of 4–11 molecules and likewise recombination is not expected or even possible if the iodine evaporates from the cluster after relaxation. On the other hand, the time scale for contact pair formation in solution is similar to that associated with the initial drop in VDE to VDE_{min} in the cluster experiments (see Fig. 4). As pointed out by Vilchiz *et al.*,[25] the contact pair in methanol does not decay to a thermalized solvated electron. Instead, the electron is initially formed in a "trapped" or "hot" state after it is injected into the liquid. The authors monitored its subsequent relaxation by shifts in the transient absorption spectrum of the electron in the spectral range of 500–700 nm. This relaxation occurred on a time scale of 10 ps for electrons in methanol, after which no further spectral evolution was observed. Spectral shifting on a similar time scale is also seen in experiments in which electrons in methanol are electronically excited.[16–18,21] In both types of experiments, this relaxation is associated with the characteristic rotational time scale of a methanol molecule in solution.[15,25,74] In the cluster experiments, we see relaxation of the VDEs on a 10 ps time scale and have attributed this process to solvent rotational motion based on consideration of initial and final states of the cluster. Hence, it appears that solvent rotation is playing a key role in relaxation phenomena seen both in solution and in our anion clusters.

VI. CONCLUSIONS

We have measured the charge-transfer-to-solvent dynamics of $I^-(CH_3OH)_n$ clusters from $n = 4$–11 with time-resolved photoelectron imaging. Vibrational autodetachment is observed to be the primary decay pathway, occurring over ~1–100 ps for this size range. The changes in the vertical detachment energies and the shapes of the spectra have been interpreted in light of newly investigated geometries of the initial and final states. Excitation of the charge transfer band leads to ejection of the excess electron from iodide onto a part of the solvent cluster, forming an unequilibrated methanol cluster anion. These clusters then relax toward the equilibrium geometry of bare anionic methanol clusters which have been shown by previous studies to have their OH bonds directed inward and their methyl groups pointing toward the surface. This relaxation is reflected in the changes in VDE and width of the excited state feature of the photoelectron spectrum and occurs over ~10–20 ps, a timescale consistent with end-over-end rotation of methanol. The contribution to the long-time destabilization from iodine loss or solvent evaporation cannot be entirely ruled out. Simulations and *ab initio* geometries would be invaluable in investigating the proposed relaxation mechanism. Complementary infrared photodissociation studies on larger $I^-(CH_3OH)_n$ ($n > 2$) would also be of use in determining the initial halide-solvent cluster geometries. Time-resolved CTTS experiments on higher alcohol clusters, specifically ethanol, will also be of interest, as these clusters should undergo a similar relaxation mechanism; these studies are currently underway in our laboratory.

ACKNOWLEDGMENTS

This work was supported by the National Science Foundation (NSF)(CHE-0649647). M.A.Y. was supported by DOD, (U.S.) Air Force Office of Scientific Research (USAFOSR), National Defense Science and Engineering Graduate (NDSEG) Fellowship, 32 CFR 168a. The authors would like to thank Professor Knut Asmis for enlightening discussions on ion microsolvation, and Markus Niemeyer for his work with our data acquisition software.

[1] E. J. Hart and M. Anbar, *The Hydrated Electron* (Wiley-Interscience, New York, 1970).
[2] J. Schnitker and P. Rossky, J. Chem. Phys. **86**, 3471 (1987).
[3] J. Jortner, M. Ottolenghi, and G. Stein, J. Phys. Chem. **68**, 247 (1964).
[4] S. E. Bradforth and P. Jungwirth, J. Phys. Chem. A **106**, 1286 (2002).
[5] X. Chen and S. E. Bradforth, Annu. Rev. Phys. Chem. **59**, 203 (2007).
[6] N. Chandrasekhar and P. Krebs, J. Chem. Phys. **112**, 5910 (2000).
[7] A. E. Bragg and B. J. Schwartz, J. Phys. Chem. B **112**, 483 (2008).
[8] A. E. Bragg and B. J. Schwartz, J. Phys. Chem. A **112**, 3530 (2008).
[9] C. Xia, J. Peon, and B. Kohler, J. Chem. Phys. **117**, 8855 (2002).
[10] M. F. Fox and E. Hayon, Chem. Phys. Lett. **25**, 511 (1974).
[11] D. Serxner, C. E. H. Dessent, and M. A. Johnson, J. Chem. Phys. **105**, 7231 (1996).
[12] L. Lehr, M. T. Zanni, C. Frischkorn, R. Weinkauf, and D. M. Neumark, Science **284**, 635 (1999).
[13] D. M. Neumark, Mol. Phys. **106**, 2183 (2008).
[14] O. T. Ehrler and D. M. Neumark, Acc. Chem. Res. **42**, 769 (2009).
[15] W. J. Chase and J. W. Hunt, J. Chem. Phys. **79**, 2835 (1975).
[16] C. Pepin, T. Goulet, D. Houde, and J.-P. Jay-Grin, J. Phys. Chem. **98**, 7009 (1994).
[17] X. Shi, F. H. Long, H. Lu, and K. B. Eisenthal, J. Phys. Chem. **99**, 6917 (1995).
[18] C. Silva, P. K. Walhout, P. J. Reid, and P. F. Barbara, J. Phys. Chem. A **102**, 5701 (1998).
[19] M. J. Tauber, C. M. Stuart, and R. A. Mathies, J. Am. Chem. Soc. **126**, 3414 (2004).
[20] T. Scheidt and R. Laenen, Chem. Phys. Lett. **371**, 445 (2003).
[21] A. Thaller, R. Laenen, and A. Laubereau, J. Chem. Phys. **124**, 024515 (2006).
[22] L. Turi, A. Mosyak, and P. Rossky, J. Chem. Phys. **107**, 1970 (1997).
[23] P. Minary, L. Turi, and P. J. Rossky, J. Chem. Phys. **110**, 10953 (1999).
[24] L. Mones and L. Turi, J. Chem. Phys. **132**, 154507 (2010).
[25] V. H. Vilchiz, X. Chen, J. A. Kloepfer, and S. E. Bradforth, Radiat. Phys. Chem. **72**, 159 (2005).
[26] C. E. H. Dessent, C. G. Bailey, and M. A. Johnson, J. Chem. Phys. **103**, 2006 (1995).
[27] W. H. Robertson, K. Karapetian, P. Ayotte, K. D. Jordan, and M. A. Johnson, J. Chem. Phys. **116**, 4853 (2002).

[28]A. V. Davis, M. T. Zanni, C. Frischkorn, and D. M. Neumark, J. Electron Spectrosc. Relat. Phenom. **108**, 203 (2000).
[29]O. M. Cabarcos, C. J. Weinheimer, T. J. Martinez, and J. M. Lisy, J. Chem. Phys. **110**, 9516 (1999).
[30]C. A. Corbett, T. J. Martinez, and J. M. Lisy, J. Phys. Chem. A **106**, 10015 (2002).
[31]J. P. Beck and J. M. Lisy, J. Phys. Chem. A **114**, 10011 (2010).
[32]R. Ayala, J. M. Martınez, R. R. Pappalardo, and E. S. Marcos, J. Phys. Chem. A **104**, 2799 (2000).
[33]L. X. Dang, J. Phys. Chem. A **108**, 9014 (2004).
[34]L. Cwiklik, G. Andersson, L. X. Dang, and P. Jungwirth, ChemPhysChem **8**, 1457 (2007).
[35]P. Jungwirth and D. J. Tobias, J. Phys. Chem. B **106**, 6361 (2002).
[36]A. Kammrath, J. R. R. Verlet, G. B. Griffin, and D. M. Neumark, J. Chem. Phys. **125**, 171102 (2006).
[37]A. Kammrath, G. B. Griffin, J. R. R. Verlet, R. M. Young, and D. M. Neumark, J. Chem. Phys. **126**, 244306 (2007).
[38]L. Mones, P. J. Rossky, and L. Turi, J. Chem. Phys. **133**, 144510 (2010).
[39]A. V. Davis, R. Wester, A. E. Bragg, and D. M. Neumark, J. Chem. Phys. **118**, 999 (2003).
[40]U. Even, J. Jortner, D. Noy, N. Lavie, and C. Cossart-Magos, J. Chem. Phys. **112**, 8068 (2000).
[41]W. C. Wiley and I. H. McLaren, Rev. Sci. Instrum. **26**, 1150 (1955).
[42]A. T. J. B. Eppink and D. H. Parker, Rev. Sci. Instrum. **68**, 3477 (1997).
[43]V. Dribinski, A. Ossadtchi, V. A. Mandelshtam, and H. Reisler, Rev. Sci. Instrum. **73**, 2634 (2002).
[44]G. A. Garcia, L. Nahon, and I. Powis, Rev. Sci. Instrum. **75**, 4989 (2004).
[45]K. L. Reid, Annu. Rev. Phys. Chem. **54**, 397 (2003).
[46]A. Kammrath, J. R. R. Verlet, A. E. Bragg, G. B. Griffin, and D. M. Neumark, J. Phys. Chem. A **109**, 11475 (2005).
[47]O. T. Ehrler, G. B. Griffin, R. M. Young, and D. M. Neumark, J. Phys. Chem. B **113**, 4031 (2009).
[48]R. Reichle, H. Helm, and I. Y. Kiyan, Phys. Rev. Lett. **87**, 243001 (2001).
[49]C. E. Klots, Z. Phys. D: At., Mol. Clusters **20**, 105 (1991).
[50]L. Ma, K. Majer, F. Chirot, and B. v. Issendorff, J. Chem. Phys. **131**, 144303 (2009).
[51]C. Frischkorn, M. T. Zanni, A. V. Davis, and D. M. Neumark, Faraday Discuss. **115**, 49 (2000).
[52]J. V. Coe, G. H. Lee, J. G. Eaton, S. T. Arnold, H. W. Sarkas, K. H. Bowen, C. Ludewigt, H. Haberland, and D. R. Worsnop, J. Chem. Phys. **92**, 3980 (1990).
[53]M. Mitsui, N. Ando, S. Kokubo, A. Nakajima, and K. Kaya, Phys. Rev. Lett. **91**, 153002 (2003).
[54]G. H. Lee, S. T. Arnold, J. G. Eaton, H. W. Sarkas, K. H. Bowen, C. Ludewigt, and H. Haberland, Z. Phys. D: At., Mol. Clusters **20**, 9 (1991).
[55]H. M. Lee, S. B. Suh, and K. Kim, J. Chem. Phys. **119**, 7685 (2003).
[56]R. A. Provencal, J. B. Paul, K. Roth, C. Chapo, R. N. Casaes, and R. J. Saykally, J. Chem. Phys. **110**, 4258 (1999).
[57]I. Natkaniec, K. Holderna-Natkaniec, I. Majerz, and K. Parlinski, Chem. Phys. **317**, 171 (2005).
[58]L. Turi, J. Chem. Phys. **110**, 10364 (1999).
[59]G. C. Pimentel and A. L. McClellan, *The Hydrogen Bond* (Reinhold, New York, 1960).
[60]R. Schinke, *Photodissociation Dynamics* (Cambridge University Press, New York, 1993).
[61]T. Iijima, J. Mol. Struct. **212**, 137 (1989).
[62]D. M. Koch and G. H. Peslherbe, Chem. Phys. Lett. **359**, 381 (2002).
[63]J. R. R. Verlet, A. E. Bragg, A. Kammrath, O. Cheshnovsky, and D. M. Neumark, Science **307**, 93 (2005).
[64]N. I. Hammer, J. W. Shin, J. M. Headrick, E. G. Diken, J. R. Roscioli, G. H. Weddle, and M. A. Johnson, Science **306**, 675 (2004).
[65]G. Markovich, L. Perera, M. L. Berkowitz, and O. Cheshnovsky, J. Chem. Phys. **105**, 2675 (1996).
[66]T. Takayanagi, J. Phys. Chem. A **110**, 7011 (2006).
[67]T. Takayanagi, Chem. Phys. **302**, 85 (2004).
[68]T. Takayanagi, J. Chem. Phys. **122**, 244307 (2005).
[69]T. Takayanagi, T. Hoshino, and K. Takahashi, Chem. Phys. **324**, 679 (2006).
[70]L. Kevan, Chem. Phys. Lett. **66**, 578 (1979).
[71]W.-S. Sheu and P. J. Rossky, J. Phys. Chem. **100**, 1295 (1996).
[72]A. Staib and D. Borgis, J. Chem. Phys. **104**, 9027 (1996).
[73]J. A. Kloepfer, V. H. Vilchiz, V. A. Lenchenkov, and S. E. Bradforth, Chem. Phys. Lett. **298**, 120 (1998).
[74]T. Goulet, C. Pepin, D. Houde, and J. P. Jay-Gerin, Radiat. Phys. Chem. **54**, 441 (1999).